SAN097-0792C
CONF-971005--3

MULTIDIMENSIONAL ELECTRON-PHOTON TRANSPORT WITH STANDARD DISCRETE ORDINATES CODES

Clifton R. Drumm

Radiation and Electromagnetic Analysis Department
Sandia National Laboratories
Albuquerque, New Mexico 87185-1166
CRDRUMM@SANDIA.GOV

Abstract

A method is described for generating electron cross sections that are compatible with standard discrete ordinates codes without modification. There are many advantages of using an established discrete ordinates solver, e.g. immediately available adjoint capability. Coupled electron-photon transport capability is needed for many applications, including the modeling of the response of electronics components to space and man-made radiation environments. The cross sections have been successfully used in the DORT, TWODANT and TORT discrete ordinates codes. The cross sections are shown to provide accurate and efficient solutions to certain multidimensional electron-photon transport problems. The key to the method is a simultaneous solution of the continuous-slowing-down (CSD) portion and elastic-scattering portion of the scattering source by the Goudsmit-Saunderson theory. The resulting multigroup-Legendre cross sections are much smaller than the true scattering cross sections that they represent. Under certain conditions, the cross sections are guaranteed positive and converge with a low-order Legendre expansion.

1. Introduction

This article describes the use of neutral-particle discrete ordinates codes for electron transport applications. Electron cross sections are computed that are compatible with standard discrete ordinates codes *without modification*. To the extent that these cross sections approximate the physics of the electron interactions, neutral-particle codes such as DORT,[1] TWODANT[2] and TORT[3] are able to model electron and coupled photon-electron-positron transport.

The advantages of such an approach are many. Adjoint capability is immediately available. Standard codes have undergone extensive benchmarking and quality assurance (QA). From a user standpoint, using the same transport code to model neutron, photon, and charged particle transport is efficient. Acceleration techniques that have been developed for neutral-particle transport apply to a certain extent to charged-particle transport.

There are also some problems involved with using a neutral-particle code for charged-particle transport. Production discrete ordinates codes are unable to model downscattering that is δ-function in angle, which is inherent in the continuous slowing down approximation (CSDA) describing charged particle transport. Furthermore, because the charged-particle interaction cross sections are generally much larger than their neutral-particle counterparts, traditional first-collision source techniques do not work well for charged-particle beams, and convergence of the solution algorithm may be slow. It is hoped, however, that the methods presented here provide some progress toward a multidimensional, deterministic electron-transport capability.

Currently, powerful Monte Carlo codes are available for electron transport.[4] While some problems are well suited for a Monte-Carlo approach, other problems are more efficiently solved with a deterministic

method, e.g. computing distributions, modeling deep penetration, and low-probability events. Still other problems are most efficiently solved with a combination of Monte Carlo and deterministic modeling. With the codes in the ITS series, one- and multi-dimensional geometries can be modeled in forward and adjoint mode, with either a continuous-energy or multigroup treatment.[5]

Deterministic electron transport capability is currently available for one-dimensional geometries, with the CEPXS/ONELD code package.[6] CEPXS/ONELD uses Gauss quadrature for slab and spherical geometries and Galerkin quadrature for cylinders. Galerkin quadrature sets are also available for multidimensional geometries.[7] However, unlike neutral-particle calculations, using standard CEPXS cross sections in neutral-particle transport codes does not allow the use of general quadrature sets.[8] The approach presented here eliminates this restriction, allowing more flexibility in the choice of quadrature sets, which is more in line with neutral-particle calculations. The CEPXS code generates cross-section libraries for coupled photon-electron-positron transport that are enough neutral-particle-like that a modified version of the ONEDANT[9] code can be used for the transport. The method relies upon remarkable ability of Gauss and Galerkin quadrature sets to exactly integrate δ-function scattering, under certain conditions. The CEPXS/ONELD code package has reached a high level of sophistication and has been used extensively for problems where one-dimensional geometry is appropriate. The approach presented here eliminates the need to exactly integrate δ-function downscattering so that general quadrature sets can be used. As described later, this is accomplished by using the Goudsmit-Saunderson theory to simultaneously solve the elastic scattering and continuous-slowing-down (CSD) components of the electron transport.

Bill Filippone and several of his students at the University of Arizona developed the multidimensional, deterministic charged-particle code, SMARTEPANTS.[10] The SMARTEPANTS code uses a different approach than the multigroup-Legendre expansion of the angle-energy dependence of the transport, an approach better suited to charged-particle interactions. The SMARTEPANTS approach is based on the Goudsmit-Saunderson solution to the infinite-medium Spencer-Lewis equation. The main limitation of this method is that the entire energy-angle-spatial down-scatter source must be kept, rather than just the scattering moments as in neutral-particle discrete-ordinates codes, so that the memory requirements are even more enormous than for traditional methods.

The work presented here combines the CEPXS/ONELD and SMARTEPANTS approaches, resulting in SMARTEPANTS-like cross sections that are compatible with neutral-particle discrete-ordinates codes. The resulting cross sections have a number of desirable properties: 1) positivity (in certain circumstances), 2) much smaller than the true interaction cross sections, 3) low-order Legendre expansion, 4) and not tied to a particular quadrature set. These desirable properties will be further explained, with limitations given, later in this article. Unlike the SMARTEPANTS code, this work is based on the Boltzmann-Fokker-Planck equation rather than the Spencer-Lewis equation (modeling based in energy rather than path length).

2. Boltzmann-Fokker-Planck Operator

The numerical modeling of electron transport is difficult because of the highly-forward-peaked nature of the scattering interactions. Electron transport is characterized by an enormous number of scattering interactions, individually having only a minimal effect on the energy and direction of travel of the electron. In other words, electron scattering cross sections are large and extremely forward peaked. Numerical methods traditionally applied to neutral-particle transport generally do not work well for modeling the transport of electrons.

For scattering that is highly forward peaked, which is characteristic of charged-particle scattering, the Legendre polynomial angular expansion of the cross sections that is normally used in discrete ordinates codes is inadequate. The electron scattering cross section is extremely forward peaked, invalidating a

standard multigroup-Legendre solution. The Boltzmann-Fokker-Planck (BFP) operator is an approximation to the Boltzmann-transport operator for scattering interactions that are highly forward peaked, such as electron transport.

In order to model electron transport with a BFP formulation, the scattering cross section is separated into three components, 1) the elastic-scattering part (for directional change without energy loss), 2) a "soft" inelastic-scattering part (for energy loss without significant directional change), and 3) a "hard" inelastic-scattering part (for both energy loss and directional change). The scattering cross section is the sum of the elastic-scattering and the "soft"-inelastic-scattering and "hard"-inelastic-scattering cross sections, where we have dropped the spatial coordinate in the cross sections,

$$\sigma_s(\mu_0, E' \rightarrow E) = \sigma_{el}(\mu_0, E) + \sigma_{in}^s(E' \rightarrow E) + \sigma_{in}^h(\mu_0, E' \rightarrow E), \tag{1}$$

where the angular dependence of the cross sections is assumed to be independent of direction, depending only upon the angle, μ_0, between the pre- and post-scattering directions of the electron. The soft-inelastic portion of the scattering cross section is approximated by the continuous slowing down approximation (CSDA),[11] so that the Boltzmann-Fokker-Planck operator is given by

$$\begin{aligned} \mathbf{L}_{BFP}\Phi(\mathbf{r}, \mathbf{\Omega}, E) = &-\mathbf{\Omega} \bullet \nabla\Phi(\mathbf{r}, \mathbf{\Omega}, E) - \left(\sigma_{el} + \sigma_{in}^h\right)\Phi(\mathbf{r}, \mathbf{\Omega}, E) \\ &+ \int \sigma_{el}(\mathbf{r}, \mu_0, E)\Phi(\mathbf{r}, \mathbf{\Omega}', E)d\mathbf{\Omega}' + \frac{\partial}{\partial E}[S\Phi] \\ &+ \iint \sigma_{in}^h(\mathbf{r}, \mu_0, E' \rightarrow E)\Phi(\mathbf{r}, \mathbf{\Omega}', E')d\mathbf{\Omega}'dE', \end{aligned} \tag{2}$$

where the stopping power is defined by

$$S(\mathbf{r}, E) = \int_E^{E+\delta} dE'\sigma_{in}^s(\mathbf{r}, E' \rightarrow E)(E - E'), \tag{3}$$

where δ is the energy boundary (artificial) between "soft" and "hard" scattering.

The inelastic-scattering cross section is separated into two components by specifying an artificial energy and directional boundary separating the two components. For energy loss greater than the artificial boundary value, the inelastic-scattering cross section is handled with a standard multigroup-Legendre expansion, requiring that this part of the cross section not be too anisotropic. For energy loss less than the artificial boundary, the inelastic-scattering cross section is modeled by the continuous-slowing-down theory, requiring that the angular change be negligible. How this boundary is specified may have a great impact on the accuracy of the result. In the CEPXS code, down scattering to an adjacent group is treated with CSD theory and down scattering beyond an adjacent group is treated with the standard multigroup-Legendre expansion. This is also the convention that is used here.

3. The Goudsmit-Saunderson Operator

The Goudsmit-Saunderson operator formulation *includes* 1) the elastic-scattering part (for directional change without energy loss), and 2) the "soft" inelastic-scattering part (for energy loss without significant directional change), and *neglects* 3) the "hard" inelastic-scattering part (for both energy loss and directional change).[12] The Goudsmit-Saunderson formulation solves the *infinite*-medium problem. The value of the Goudsmit-Saunderson equation is that it can be solved exactly. The Goudsmit-Saunderson operator is

$$\mathbf{L}_{GS}\Phi(\mathbf{\Omega}, E) = -\sigma_{el}\Phi(\mathbf{\Omega}, E) + \int \sigma_{el}(\mu_0, E)\Phi(\mathbf{\Omega}', E)d\mathbf{\Omega}' + \frac{\partial}{\partial E}[S\Phi] \tag{4}$$

The Goudsmit-Saunderson solution is based upon the expansion of the angular fluence and elastic-

scattering cross section in infinite Legendre-polynomial expansions. The elastic-scattering cross section is extremely forward peaked and, therefore, requires a huge number of Legendre expansion coefficients for accurate modeling (typically ~200). If the angular fluence and the elastic scattering cross section are expanded in infinite Legendre-polynomial series. The angular fluence at energy E is, after some manipulation, related to the angular fluence at an upper energy bound, $\Phi(\mu, E_0)$, by

$$S(E)\Phi(\mu,E) = \sum_{n=0}^{\infty} \frac{2n+1}{2} \int d\mu' P_n(\mu) e^{-\int_E^{E_0} dE' \left(\frac{\sigma_{el}^0 - \sigma_{el}^n}{S}\right)} P_n(\mu') S(E_0)\Phi(\mu', E_0). \quad (5)$$

Eq. (5) forms the basis of the current method. To summarize, Eq. (5) relates the angular fluence at a given energy, E, to the integral over angle of the angular fluence at a higher energy, E_0, neglecting "hard" scattering and spatial effects.

The Goudsmit-Saunderson approach combines the elastic scattering and continuous slowing down in a single downscatter operator. The success of the method depends on this downscatter operator being less anisotropic than the scattering cross section. The anisotropy of the downscatter operator is related to the separation between the two energy bounds, E and E_0. Referring to Eq. (5), as E_0 approaches E, the exponential term in Eq. (5) vanishes, and the downscatter operator approaches a δ function. Conversely, as the separation between the two energy bounds increases, the downscatter operator becomes less anisotropic, due to the presence of the exponential term. Physically the reason for this is that as the electrons slow down from E_0 to E, the elastic scattering deflects the electrons.

The elastic-scattering cross section is extremely forward peaked, but the Goudsmit-Saunderson expansion removes a δ-function component from the elastic scattering cross section, utilizing only the difference between the moments of the elastic-scattering cross section rather than the moments themselves (δ-function elastic scattering is like no scattering at all, and can be removed without effect). By combining the CSD with the non-δ-function component of the elastic scattering, the down scattering is much less forward peaked, and may be approximated by a low-order Legendre expansion.

The multigroup-Legendre solution, of the type used by standard discrete-ordinates codes, of the Goudsmit-Saunderson is

$$\sigma_{t,g}\Phi_g(\mu) = \sum_{g'=1}^{G} \sum_{l=0}^{L} \frac{2l+1}{2} \int d\mu' P_l(\mu) \sigma_{g'\to g}^l P_l(\mu') \Phi_{g'}(\mu'), \quad (6)$$

where $\sigma_{g'\to g}^l$ are the moments of the multigroup scattering cross sections. Comparing Eqs. (6) and (5) suggests that it may be possible to approximate the Goudsmit-Saunderson downscatter operator by multigroup-Legendre cross sections. Integrating Eq. (5) over energy group g and dividing by the group width, and truncating the Legendre expansion at the Lth moment, results in an equation that is very similar to the multigroup-Legendre solution,

$$\frac{S_g}{\Delta E_g}\Phi_g(\mu) = \int d\bar{\mu}' \left\{ \frac{1}{2} + \sum_{l=1}^{L} \left(\frac{2l+1}{2}\right) P_l(\mu) e^{-\int_{E_{g-\frac{1}{2}}}^{E_0} dE' \left(\frac{\sigma_{el}^0 - \sigma_{el}^l}{S}\right)} \right.$$

$$\left. \left(\frac{S_g/\Delta E_g}{\sigma_g^0 - \sigma_g^l}\right) \left[1 - e^{-\left(\frac{\sigma_g^0 - \sigma_g^l}{S_g}\right)\Delta E_g}\right] P_l(\mu') \right\} S(E_0)\Phi(\mu', E_0). \quad (7)$$

$\Phi(\mu, E_0)$ is the angular fluence at as yet unspecified energy E_0. In the following sections, $\Phi(\mu, E_0)$ will be related to the multigroup angular fluences, resulting in several different forms of the multigroup-Legendre scattering moments.

4. Multigroup-Legendre Cross Sections

Eq. (7) relates the group-g multigroup fluence to the fluence at an upper energy bound, E_0. In order to proceed, a relationship between the multigroup and boundary fluences is needed. The nature of this relationship has a profound effect on the properties of the resulting multigroup-Legendre cross sections and on the accuracy of the approximation. In this section, two different energy-differencing approximations are described. The first is a linear-continuous (diamond) differencing, which is very accurate, but results in negative cross sections. The second differencing method results in all positive cross section, but with some loss in accuracy.

4.1 Linear-Continuous Differencing

The linear-continuous (diamond-difference) approximation is illustrated in Fig. 1, which shows the relationship between the multigroup values (dashed lines) and continuous values (solid lines).

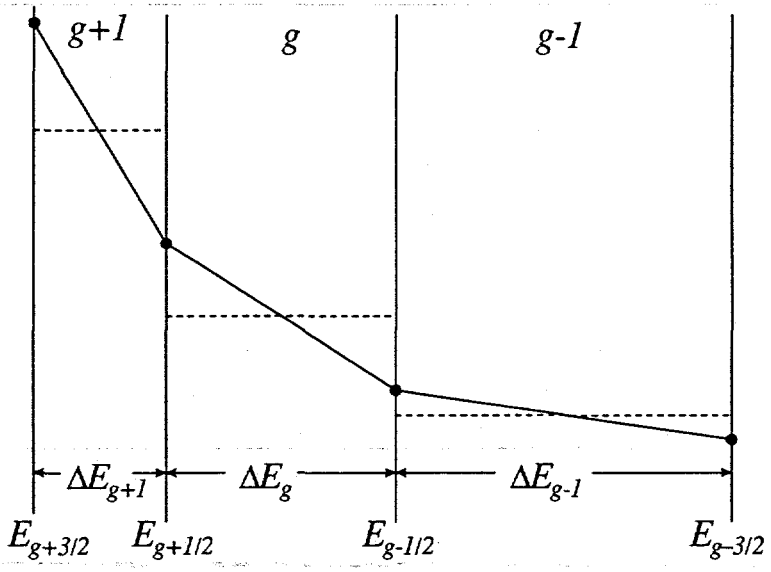

Figure 1: Linear-continuous differencing showing the relationship between the differential and multigroup values.

Utilizing a linear-continuous approximation in Eq. (7), after some manipulation,[13] results in total, downscatter, and absorption cross sections,

$$\sigma_{t,g} = 2\frac{S_g}{\Delta E_g},\ \sigma^0_{g\to g'} = 4(-1)^{g-g'-1}\frac{S_g}{\Delta E_g},\ \text{and}\ \sigma_{a,g} = 2(-1)^{G-g}\frac{S_g}{\Delta E_g}. \tag{8}$$

Unlike the standard CEPXS cross sections, the self-scatter cross sections are all zero, and the higher-order down-scatter moments are

$$\sigma^l_{g\to g'} = \sigma^0_{g\to g'}\left(\frac{S_{g'}/\Delta E_{g'}}{\sigma^0_{g'} - \sigma^l_{g'}}\right)\left[1 - e^{-\left(\frac{\sigma^0_{g'}-\sigma^l_{g'}}{S_{g'}}\right)\Delta E_{g'}}\right]. \tag{9}$$

This method results in cross sections that are very effective for modeling integral quantities, such as charge and energy deposition profiles. The cross sections are not tied to a particular quadrature set. The cross sections are also much smaller than the true scattering interactions that they represent, resulting in

fast convergence of the discrete-ordinates solutions.

The cross sections also have some undesirable features, however, including 1) many negative cross section elements, and 2) the cross sections may result in severe oscillations in the energy dependence of the calculated fluence. The energy differencing scheme described in the next section eliminates these undesirable features, but with some loss of accuracy.

4.2 First-Order Polynomial Differencing

A first-order polynomial approximation results in total, self- and down-scatter, and absorption cross sections given by

$$\sigma_{t,g} = 2\frac{S_g}{\Delta E}, \text{ and } \sigma^0_{g\to g} = \sigma^0_{g\to g+1} = \sigma_{a,G} = \frac{S_G}{\Delta E}. \tag{10}$$

The higher-order scatter moments are as before

$$\sigma^l_{g\to g'} = \sigma^0_{g\to g'}\left(\frac{S_{g'}/\Delta E_{g'}}{\sigma^0_{g'} - \sigma^l_{g'}}\right)\left[1 - e^{-\left(\frac{\sigma^0_{g'}-\sigma^l_{g'}}{S_{g'}}\right)\Delta E_{g'}}\right]. \tag{11}$$

This procedure results in a multigroup-Legendre cross sections that are all positive that work well in the DORT code. The cross sections are less accurate for computing energy deposition profiles than are the linear-continuous cross sections due to numerical straggling, which is the artificial spreading of the energy dependence resulting from the multigroup approximation.

5. Summary and Comparison with Measurements and Monte Carlo Calculations

The Goudsmit-Saunderson approach combines the elastic scattering and CSD terms into a single down-scatter cross section. By averaging over energy groups, the need to model δ-function downscattering is eliminated, and the downscatter cross section can be approximated by a truncated Legendre-expansion. In this section we demonstrate good agreement with experiment and Monte Carlo results for several test problems.

The cross sections were computed with a version of the CEPXS[8] code, modified to include the Goudsmit-Saunderson terms in the cross sections. The CEPXS code produces a cross section library in the BXSLIB format that is directly usable in the ONELD[9] code, which was used for the one-dimensional calculations. The CEPXS cross sections were further processed into the GIP format for use in the DORT[1] code, which was used for the two-dimensional simulations. The DORT calculations used θ-weighted spatial differencing and an S-16 fully symmetric quadrature set.

The discrete-ordinates results are compared with measurements, when available. For problems where measurements are not available, the discrete-ordinates results are compared with Monte Carlo calculations performed with the ITS[4] codes. The TIGER code of the ITS package was used for the 1-dimensional calculations, and the ACCEPT code, which has combinatorial-geometry modeling capability, was used for the 2-dimensional calculations. The accuracy of the discrete-ordinates results depends on the fineness of the discretization (spatial mesh, energy grid, and angular quadrature order) used in the calculation. The discretizations were refined to the point where further refinement resulted in only a few percent change in the results. Uniform energy groups were used for all of the calculations.

All of the discrete-ordinates calculations and most of the Monte Carlo calculations were performed on a single processor of a SUN-SPARC1000 workstation. The single exception to this was the ACCEPT modeling of the junction-diode electron-hole pair distribution described in Sec. 5.1.3, which was performed with 1,000 processors on a PARAGON. This modeling was done on the PARAGON, since the estimated

SUN-SPARC1000 runtime was about 60 days.

5.1 Energy-Deposition Profiles

5.1.1 One-dimensional measurements of Lockwood et al.

Lockwood, et al.[14] have used a calorimetric technique to measure energy-deposition profiles in one-dimensional geometries for electron sources. They used electron beams with energies ranging from 0.3 to 1.0 MeV, and they considered targets ranging from low-Z elements such as beryllium to high-Z elements such as uranium. They also measured energy deposition profiles for several high-Z/low-Z multilayer arrangements. The reported experimental uncertainties are less than a few percent.

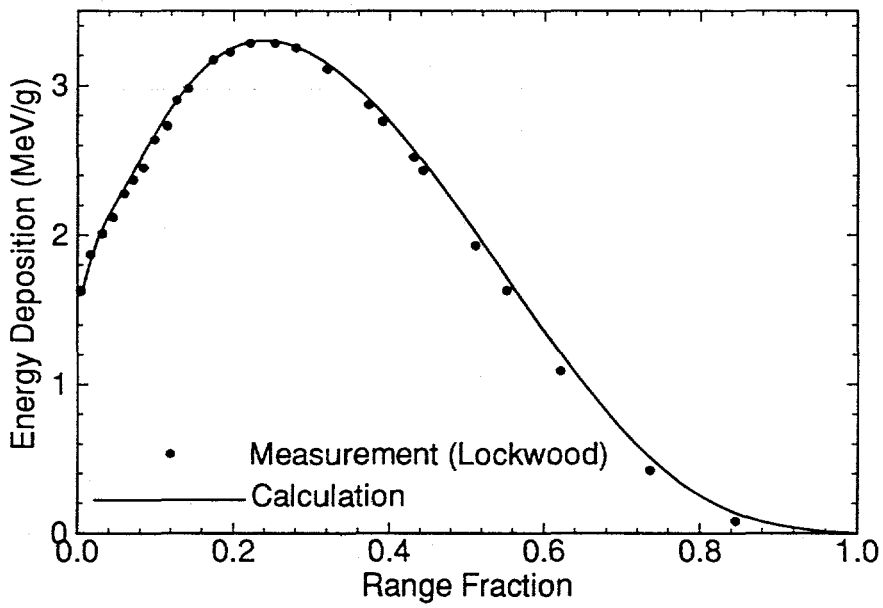

Figure 2: Comparison of discrete-ordinates calculation with the measurement of energy deposition versus depth for 1-MeV electrons normally incident on aluminum. Electrons are incident from the left. Depth is given in terms of the fraction of an electron range.

We have modeled several of the Lockwood geometries with the CEPXS-GS/ONELD codes. For 1-MeV, normally-incident electrons on aluminum, the results are shown in Fig. 2. The CEPXS-GS/ONELD calculation used 50 electron energy groups, S-32 Gauss quadrature, P-11 Legendre expansion, and required 0.9 min on a SPARC1000 processor. The calculation and measurement are in excellent agreement.

5.1.2 1-MeV electron beams on two-dimensional tantalum

Figs. 3 and 4 are plots of the Monte Carlo and discrete ordinates calculations of energy-deposition distributions for a 1-MeV collimated electron beam normally incident on a bar of tantalum that is 0.015 by 0.015 cm (about one third of a range thick). The electron beam is collimated to a width of 6 μm, normalized to one source electron. The modeling is done in two dimensions, implying an infinite length in one of the axes. The CEPXS-GS/DORT calculation used 2,500 spatial cells (50x50), 100 electron energy groups, S-16 quadrature, and P-5 Legendre expansion, and required 282 minutes on a SPARC1000 processor. The agreement between Monte Carlo and discrete-ordinates is very good. The Monte Carlo results are

less-smooth, due to the statistical nature of the solution.

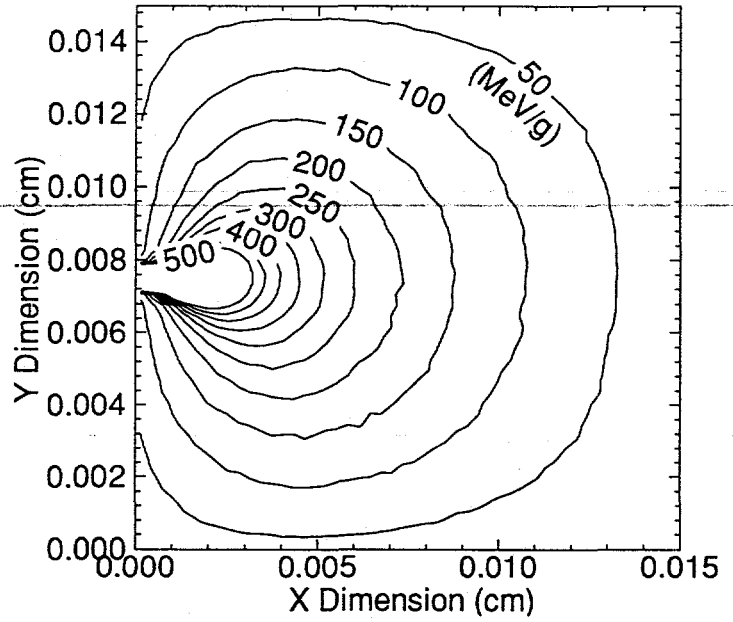

Figure 3: Monte Carlo calculation of the energy-deposition contours from a collimated beam of 1-MeV electrons normally incident on tantalum.

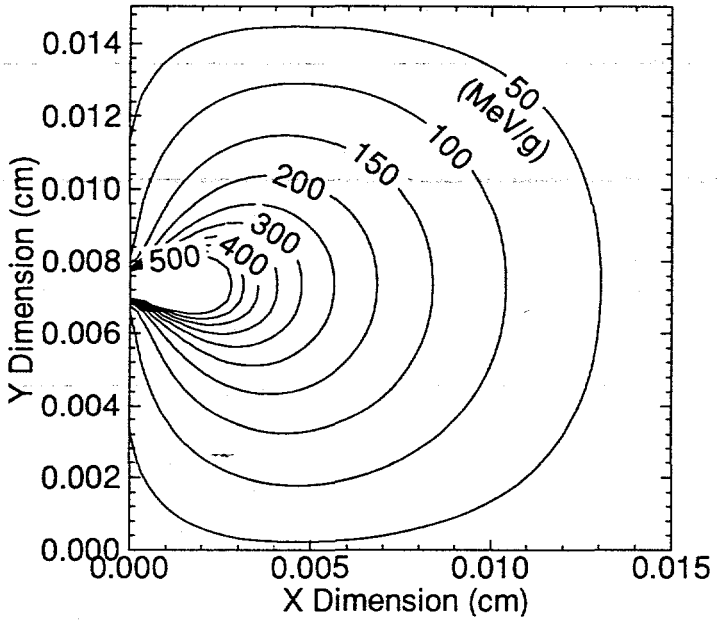

Figure 4: Discrete-ordinates calculation of the energy-deposition contours from a collimated beam of 1-MeV electrons normally incident on tantalum.

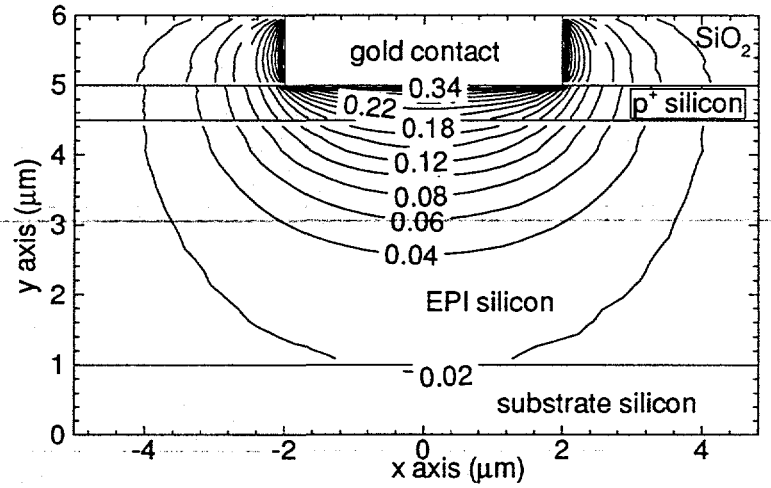

Figure 5: Monte Carlo modeling of the electron-hole-pair distribution from 100-keV photons normally incident a gold-contact diode. Photons are incident from the top and are normalized to 1 erg/cm^2. The contours are electron-hole pairs per cubic micrometer.

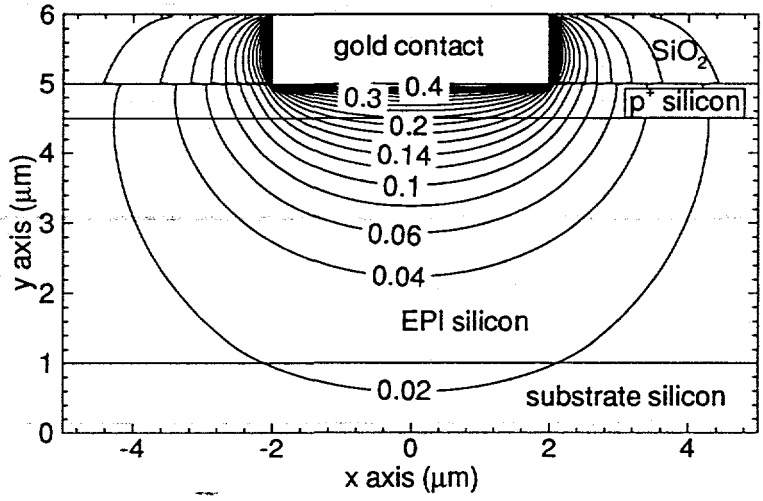

Figure 6: Discrete-ordinates modeling of the electron-hole-pair distribution from 100-keV photons normally incident a gold-contact diode. Photons are incident from the top and are normalized to 1 erg/cm^2. The contours are electron-hole pairs per cubic micrometer.

5.1.3 Junction-diode electron-hole pair distribution

The response of semiconductor devices (such as junction diodes) to irradiation depends upon the distribution of electron-hole pairs throughout the semiconductor materials. The cross section of a typical junction

diode is shown in Fig. 5. The diode consists of a thin (1 μm by 4 μm) gold contact adjacent to a 0.5-μm p^+ silicon layer, followed by a 3.5-μm EPI silicon layer, above substrate silicon.

Figs. 5 and 6 show the distribution of electron-hole pairs for 100-keV photons normally incident from the top of the junction diode. Fig. 5 shows the ACCEPT results and Fig. 6 shows the CEPXS-GS/DORT results. A P-3 Legendre expansion is adequate to model the scattering, because the electrons production is fairly diffuse in angle. The photon source was normalized to 1 erg/cm^2, and the electron-hole pair distributions are shown in units of electron-hole pairs per cubic micrometer.

The generation of electron-hole pairs is dominated by electron emission from the gold contact into the surrounding semiconductor materials. The electron-hole pair distribution was computed from the energy-deposition distribution, assuming 3.6 eV per electron-hole pair. The discrete-ordinates results are about 10% higher than the corresponding Monte Carlo results. The reason for this difference is not understood, but the difference does persist with a finer energy and angle discretization and with a higher-order Legendre expansion of the scattering. The CEPXS-GS/DORT calculation used 5,400 spatial cells, 40 photon energy groups and 100 electron energy groups, S-16 quadrature, P-3 Legendre expansion, and required 142 minutes on a SPARC1000 processor.

5.2 Electron-Emission Spectra

5.2.1 Electron beam on two-dimensional tantalum

Fig. 7 shows the reflected, transmitted, and transverse electron spectra emitted from the one–third range tantalum bar irradiated with a collimated beam of 1-MeV electrons, described in Sec. 5.1.2. The symbols are the ACCEPT results and the smooth curves are the CEPXS-GS/DORT results. The agreement is quite good, differing by at most about five percent. The only exception to this is at the very low energy end of the spectrum, where the discrete-ordinates results of the reflected spectra is much higher than the Monte Carlo results. The reason for this difference is not known.

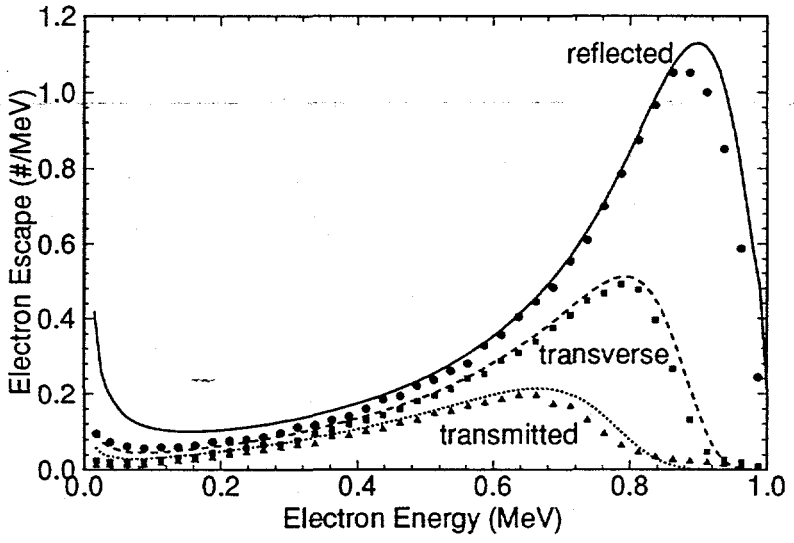

Figure 7: Electron-emission spectra from a 1-MeV electron beam incident on a two-dimensional, one-third electron range tantalum. The symbols are the ACCEPT Monte Carlo results and the smooth curves are the discrete-ordinates results. The reflected, transmitted, and transverse spectra are shown.

6. Discussion and Suggestions for future work

The multigroup-Legendre cross sections also work well in adjoint calculations, and there are many potential applications in this area. The cross sections should also be effective for multigroup Monte Carlo calculations.

The multigroup-Legendre cross sections have been demonstrated to work for a wide variety of problems. However, there are some problems for which the cross sections have not worked so well. For high-energy electron beams on water (of importance in radiation oncology studies) a very high-order Legendre expansion is required. For these types of problems some type of first-collision source technique may prove effective.[15] For high-energy electron beams on high-Z materials a large number of energy groups is required to reduce numerical straggling. Allowing for non-uniform electron energy group widths would improve the modeling, in some cases.

The use of CEPXS-GS cross sections eliminate well-known numerical oscillations in the CEPXS/ONELD results in some cases with a very small spatial mesh size. As described on p. 44 of the CEPXS results guide,[6] energy-deposition profiles can oscillate severely for a monoenergetic electron beam incident on a low-Z material. Fig. 8 shows that these oscillations are eliminated by using CEPXS-GS cross sections. Fig. 8 shows the energy-deposition profiles for 1-MeV electrons normally incident on one-dimensional beryllium. The calculations used an cutoff energy of 0.01 MeV, 200 spatial meshes, 40 electron energy groups, and an S-32 Gauss quadrature set. The CEPXS/ONELD calculation used a P-31 Legendre expansion, and the CEPXS-GS/ONELD calculation used a P-17 Legendre expansion.

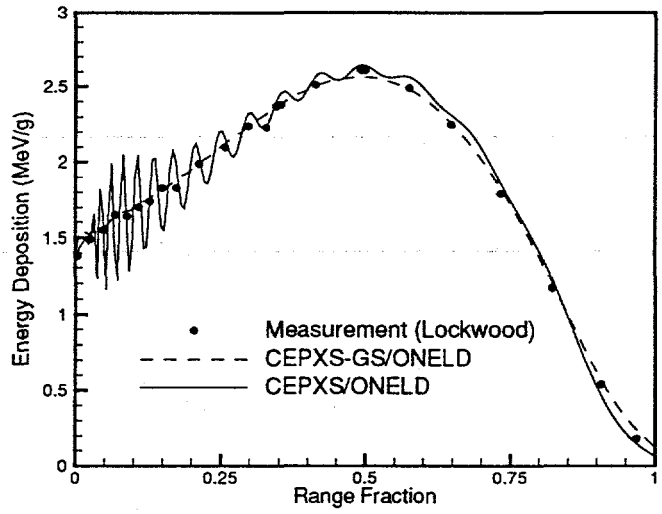

Figure 8: Comparison of CEPXS-GS/ONELD, standard CEPXS/ONELD, and Lockwood measurements for 1-MeV electrons normally incident on range-thick beryllium.

Acknowledgments

Thanks is expressed to Wesley Fan for many helpful discussions relating to this work and for performing the ACCEPT modeling on the PARAGON computer. Thanks is also expressed to Len Lorence for many helpful discussions regarding the CEPXS cross sections. This work was supported by the U.S. Department

of Energy Contract DE-AC04-94-AL85000. Sandia is a multiprogram laboratory operated by Sandia Corporation, a Lockheed Martin Company, for the United States Department of Energy.

7. REFERENCES

[1] W. A. Rhoades and R. L. Childs, "An Updated Version of the DOT 4 One- and Two-Dimensional Neutron/Photon Transport Code," Oak Ridge National Laboratory Report, ORNL-5851 (1982).

[2] R. E. Alcouffe, et al., "User's Guide for TWODANT: A Code Package for Two-Dimensional, Diffusion-Accelerated, Neutral-Particle Transport," Los Alamos National Laboratory Report, LA-10049-M, Rev. 1 (1990).

[3] W. A. Rhoades and R. L. Childs, "The TORT Three-Dimensional Discrete Ordinates Neutron/Photon Transport Code," Oak Ridge National Laboratory Report, ORNL-6268 (1987).

[4] J. A. Halbleib, R. P. Kensek, G. D. Valdez, S. M. Seltzer and M. J. Berger, "ITS: The Integrated TIGER Series of Coupled Electron/Photon Monte Carlo Transport Codes - Version 3.0," *IEEE Trans. Nucl. Sci.*, **39**, 1025 (1992).

[5] J. E. Morel, L. J. Lorence, Jr., R. P. Kensek, J. A. Halbleib, and D. P. Sloan, "A Hybrid Multigroup/Continuous Energy Monte Carlo Method for Solving the Boltzmann Fokker Planck Equation," *Nucl. Sci. Eng.*, **124**, 369 (1996).

[6] L. J. Lorence, Jr., J. E. Morel, and G. D. Valdez, "Results Guide to CEPXS/ONELD: A One-Dimensional Coupled Electron-Photon Code Package Version 1.0," Sandia National Laboratories report, SAND89-2211 (1990).

[7] J. E. Morel, "A Hybrid Collocation-Galerkin-S_n Method for Solving the Boltzmann Transport Equation," *Nucl. Sci. Eng.*, **101**, 72 (1989).

[8] L. J. Lorence, Jr., J. E. Morel, and G. D. Valdez, "Physics Guide to CEPXS: A Multigroup Coupled Electron-Photon Cross-Section Generating Code," Sandia National Laboratories report, SAND89-1685 (1989).

[9] R. D. O'Dell, et al., "Revised User's Manual for ONEDANT: A Code Package for One-Dimensional, Diffusion-Accelerated, Neutral-Particle Transport," Los Alamos National Laboratory Report, LA-9184-M, Rev. (1989).

[10] W. L. Filippone, "The Theory and Application of SMART Electron Scattering Matrices," *Nucl. Sci. Eng.*, **99**, 232 (1988).

[11] J. E. Morel, "Fokker-Planck Calculations Using Standard Discrete Ordinates Transport Codes," *Nucl. Sci. Eng.*, **79**, 340 (1981).

[12] S. Goudsmit and J. L. Saunderson, "Multiple Scattering of Electrons," *Phys. Rev.* **57**, 24 (1940).

[13] J. E. Morel, "Multigroup Legendre Coefficients for the Diamond Difference Continuous Slowing Down Operator," *Nucl. Sci. Eng.*, **91**, 324 (1985).

[14] G. J. Lockwood, L. E. Ruggles, G. H. Miller, and J. A. Halbleib, "Calorimetric Measurement of Electron Energy Deposition in Extended Media – Theory vs Experiment," Sandia National Laboratories report, SAND79-0414 (1979).

[15] W. L. Filippone, J. E. Morel, and W. F. Walters, "An Extended First Collision Source Method for Electron Beam Source Problems," *Nucl. Sci. Eng.*, **112**, 1 (1992).